GDCh

Communications

Angewandte
Chemie
International Edition
www.angewandte.org

Silver Clusters

Elucidating the Structures of Intermediate Fragments during Stepwise Dissociation of Monolayer-Protected Silver Clusters

Papri Chakraborty,* Sami Malola, Marco Neumaier, Patrick Weis, Hannu Häkkinen,* and Manfred M. Kappes*

Abstract: Fragmentation dynamics of ligated coinage metal clusters reflects their structural and bonding properties. So far methodological challenges limited probing structures of the fragments. Herein, we resolve the geometric structures of the primary fragments of $[Ag_{29}L_{12}]^{3-}$, i.e. $[Ag_{24}L_9]^{2-}$, $[Ag_{19}L_6]^-$ and $[Ag_5L_3]^-$ (L is 1,3-benzene dithiolate). For this, we used trapped ion mobility mass spectrometry to determine collision cross sections of the fragments and compared them to structures calculated by density functional theory. We also report that following two sequential $[Ag_5L_3]^-$ elimination steps, further dissociation of $[Ag_{19}L_6]^-$ also involves a new channel of Ag_2 loss and Ag–S and C–S bond cleavages. This reflects a competition between retaining the electronic stability of $8e^-$ superatom cluster cores and increasing steric strain of ligands and staples. These results are also of potential interest for future soft-landing deposition studies aimed at probing catalytic behavior of Ag clusters on supports.

Atomically precise coinage metal clusters, protected by a monolayer of thiolate ligands, are of growing interest due to their diverse structures, properties and applications.[1] Gas-phase dissociation reactions can provide information on cluster size-dependent thermodynamic properties and have

thus been extensively studied. Fragmentation can be induced through techniques such as collision induced dissociation (CID),[2] surface induced dissociation[3] or UV photodissociation.[4] The most studied cluster, $[Au_{25}(SR)_{18}]^{\pm}$ (SR is a thiolate)[5] loses neutral $Au_4(SR)_4$ units in the gas phase and correspondingly produces large fragmented cluster ions like $[Au_{21}(SR)_{14}]^{\pm}$, $[Au_{17}(SR)_{10}]^{\pm}$ etc.[2b,6] Fragmentation of thiolate-protected Ag clusters also results in loss of smaller units like $Ag_5(SR)_6$, $Ag(SR)_2$ etc.[2a] A prime example is $[Ag_{29}L_{12}]^{3-}$ (L is 1,3-benzene dithiolate, i.e., BDT) for which collisional activation produces $[Ag_{24}L_9]^{2-}$ and $[Ag_{19}L_6]^-$ through the concomitant loss of $[Ag_5L_3]^-$.[2a] Although, the molecular composition of these fragments has been established from mass spectrometry (MS), there is no information about their structures. Herein, we studied the fragmentation of $[Ag_{29}L_{12}]^{3-}$ through a combination of CID and trapped ion mobility spectrometry (TIMS)[7] coupled with MS. Here, the collision cross-sections (CCSs) of parent $[Ag_{29}L_{12}]^{3-}$ *and its fragment ions* $[Ag_{24}L_9]^{2-}$, $[Ag_{19}L_6]^-$ and $[Ag_5L_3]^-$ were measured by TIMS MS. These CCS values allowed an assignment of the ion geometries by comparison to density functional theory (DFT) calculations of plausible model structures.

Ion mobility (IM) MS, in combination with theoretical calculations, has been extensively used earlier to assign gas-phase structures of large biomolecules, clusters, proteins, etc.[8] Often the method has been validated by X-ray crystallography. For example, C_{60}^- showed $^{TIMS}CCS_{N2}$ of 211.6 Å^2 and the calculated CCS agreed within ≈1%. Similar results were also observed for higher fullerenes and endohedral metallofullerenes.[9] IM MS has also been recently applied to explore possible isomeric structures of coinage metal clusters in the gas-phase[10] and to follow their structural changes during chemical reactions.[2b,11] Also for this compound class the reliability of IM MS based structure assignment has been evidenced in the literature by being applied to ligand-protected metal nanoclusters with known X-ray structures. For $[Ag_{14}(C\equiv CtBu)_{12}Cl]^+$, $[Ag_8Cu_6(C\equiv CtBu)_{12}Cl]^+$, $[Ag_{14}(C\equiv CtBu)_{12}Br]^+$ and $[Ag_8Cu_6(C\equiv CtBu)_{12}Br]^+$, uniformly good agreement between experimental and calculated CCS was observed.[12] Furthermore, Soleilhac et al. also used IM MS to determine CCSs of a series of gold clusters, protected by glutathione, and showed that the relative changes in CCSs of these clusters in the gas-phase were consistent with the relative changes in size predicted by X-ray powder diffraction in the solid state and by time-resolved fluorescence anisotropy in the solution phase.[13] Gas-phase structures of several clusters like Au$_7$-

[*] Dr. P. Chakraborty, Dr. M. Neumaier, Prof. M. M. Kappes
Institute of Nanotechnology, Karlsruhe Institute of Technology
76344 Eggenstein-Leopoldshafen (Germany)
E-mail: pc.paprichakraborty@gmail.com
        manfred.kappes@kit.edu

Dr. P. Chakraborty, Dr. P. Weis, Prof. M. M. Kappes
Institute of Physical Chemistry, Karlsruhe Institute of Technology
76131 Karlsruhe (Germany)

Dr. S. Malola, Prof. H. Häkkinen
Department of Physics, Nanoscience Center, University of Jyväskylä
40014 Jyväskylä (Finland)
E-mail: hannu.j.hakkinen@jyu.fi

Prof. H. Häkkinen
Department of Chemistry, Nanoscience Center, University of Jyväskylä
40014 Jyväskylä (Finland)

$(PPh_3)_7H_5^{2+}$ and $Au_8(PPh_3)_7^{2+}$ were also assigned based on the agreement of experimental and calculated CCS.[14] TIMS MS, in combination with DFT, was used to resolve small changes in CCS resulting from Cu doping in different positions of $[Ag_{29}(BDT)_{12}]^{3-}$ cluster.[11b]

In the present study, $[Ag_{29}L_{12}]^{3-}$, synthesized using a reported method[15] (see Supporting Information), was characterized by electrospray ionization MS (Figure S1). CID of $[Ag_{29}L_{12}]^{3-}$ (m/z 1603) generates the fragment ions $[Ag_{24}L_9]^{2-}$ (m/z 1924), $[Ag_{19}L_6]^-$ (m/z 2888) and $[Ag_5L_3]^-$ (m/z 960) as normalized collision energy (NCE) is increased (Figure 1A, S2A). Isolation of the primary $[Ag_{24}L_9]^{2-}$ fragment and subsequent CID thereof results in the formation of $[Ag_{19}L_6]^-$ and $[Ag_5L_3]^-$ (Figure S2B) thus confirming the stepwise elimination of $[Ag_5L_3]^-$ from $[Ag_{29}L_{12}]^{3-}$ which was not explicitly observed in earlier reports.[2a] CID of isolated $[Ag_{19}L_6]^-$ shows some further $[Ag_5L_3]^-$ loss to form presumably neutral $[Ag_{14}L_3]$. However, in contrast to $[Ag_{29}L_{12}]^{3-}$ and $[Ag_{24}L_9]^{2-}$ which fragment only by $[Ag_5L_3]^-$ elimination, $[Ag_{19}L_6]^-$ undergoes mainly Ag_2 loss resulting in $[Ag_{17}L_6]^-$, $[Ag_{15}L_6]^-$ and $[Ag_{13}L_6]^-$ (Figure 1B). At even higher collision energies, extensive cleavage of the Ag–Ag, Ag–S and C–S bonds leads to complete dissociation of $[Ag_{19}L_6]^-$ (Figure S3). To gauge the structural changes during the stepwise dissociation of the cluster, TIMS MS studies on parent $[Ag_{29}L_{12}]^{3-}$ cluster and its fragment ions, $[Ag_{24}L_9]^{2-}$, $[Ag_{19}L_6]^-$ and $[Ag_5L_3]^-$, were performed using a Bruker TIMS TOF instrument. Here, fragmentation of $[Ag_{29}L_{12}]^{3-}$ was achieved by varying the ion transmission voltages ($\Delta6$) in the range of -100 V to -200 V (Figure S4), that acts on the ions prior to the IM separation. This method of ion activation in the TIMS setup has been previously established

for other systems.[16] A comparison of experimental versus calculated isotopic patterns for the fragment ions thus confirming their compositional assignment is shown in Figure S5. Figure 2A shows TIMS measurements of the parent and the fragment ions under different voltage conditions, which revealed single peak mobilograms with corresponding CCSs independent of activation conditions (Figure S6) thus indicating stable structures for the ions. $^{TIMS}CCS_{N2}$ of parent $[Ag_{29}L_{12}]^{3-}$ was 476 Å^2 which is consistent with the recently reported value.[11b] $^{TIMS}CCS_{N2}$ of the larger fragments $[Ag_{24}L_9]^{2-}$ and $[Ag_{19}L_6]^-$ were 383 and 303 Å^2, respectively, and the smaller $[Ag_5L_3]^-$ fragment was 212 Å^2. (Note that TIMS mobilograms are deconvoluted from mass spectral information, i.e. refer to specific m/z values and isotopic patterns; hence the experimental ^{TIMS}-CCS_{N2} values corresponds only to the species indicated). A schematic of the two-step fragmentation pathway to form $[Ag_{19}L_6]^-$ is presented in Figure 2B. As we observed a single peak in TIMS for each of the parent and fragment ions, coexistence of multiple isomers for a particular species is unlikely, except that the isomers have similar CCS within the resolution limit of the TIMS measurement.

The structures of the parent and the fragment ions were next investigated by DFT using the GPAW[17] package with Perdew–Burke–Ernzerhof (PBE) exchange-correlation (xc) functional.[18] Theoretical CCS of the calculated structures were determined using the trajectory method (TM) in IMoS 1.09 package.[19] Further details on the computational methods are in Supporting Information. The crystal structure of $[Ag_{29}L_{12}]^{3-}$ cluster consists of an icosahedral core and 16 Ag atoms in the outer staples (staples consist of Ag–S motifs surrounding the core), covered by 12 BDT ligands.[15]
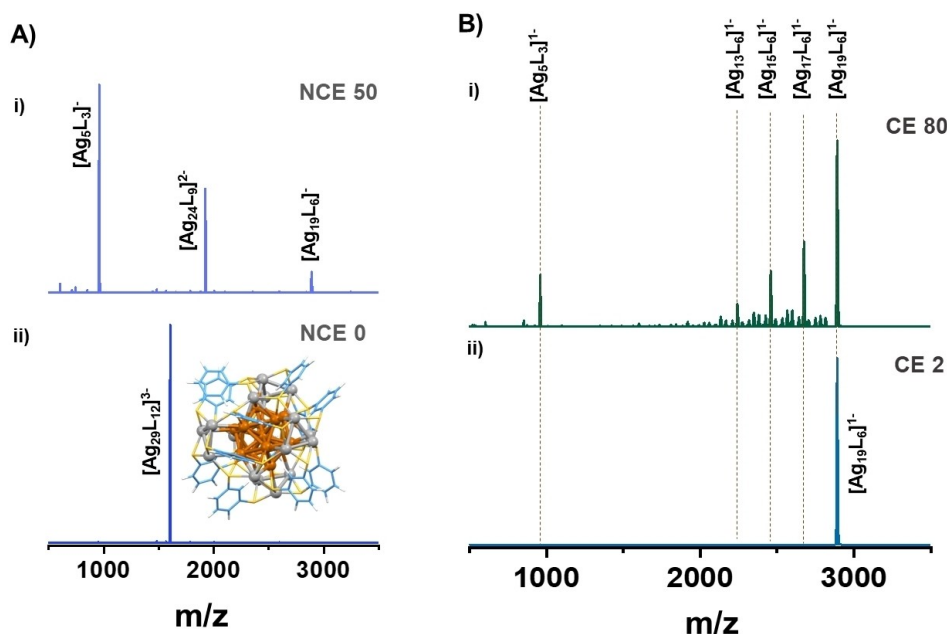

Figure 1. A) CID of $[Ag_{29}L_{12}]^{3-}$ at i) NCE 50, ii) NCE 0. Note dominant $[Ag_5L_3]^-$ loss to yield $[Ag_{24}L_9]^{2-}$. $[Ag_{24}L_9]^{2-}$ also fragments via dominant $[Ag_5L_3]^-$ loss to yield $[Ag_{19}L_6]^-$ (see Figure S2). B) CID of $[Ag_{19}L_6]^-$ at i) CE 80, ii) CE 2 (L=1,3-BDT) shows mainly two parallel fragmentation channels (some $[Ag_5L_3]^-$ and mainly Ag_2 loss). The structure of the $[Ag_{29}L_{12}]^{3-}$ precursor is presented in inset of A,ii. Colour: Ag (orange: core, grey: staple), S (yellow), C (blue) and H (white).
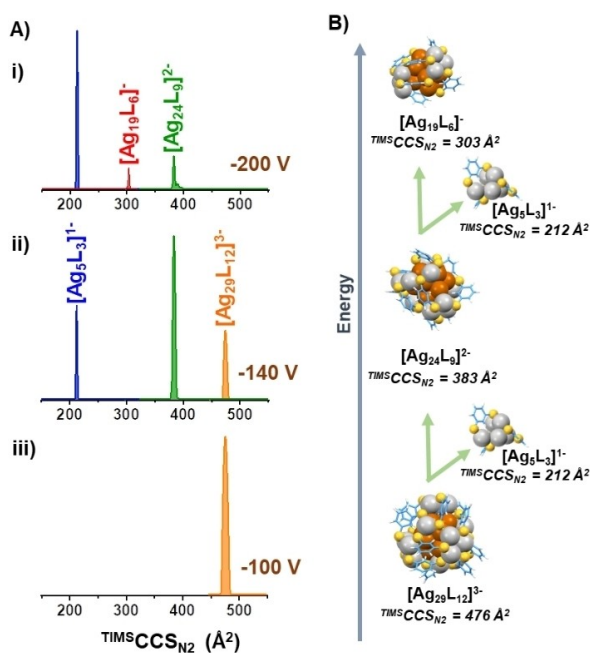
Figure 2. A) TIMS MS of $[Ag_{29}L_{12}]^{3-}$ and its fragments $[Ag_{24}L_9]^{2-}$, $[Ag_{19}L_6]^-$ and $[Ag_5L_3]^-$ at $\Delta 6$ voltage of i) -200 V, ii) -140 V and iii) -100 V. B) Scheme of the two-step fragmentation of $[Ag_{29}L_{12}]^{3-}$ to $[Ag_{19}L_6]^{1-}$ (L=1,3-BDT).

DFT optimized structure of $[Ag_{29}L_{12}]^{3-}$ (Figure 1Aii) yielded $^{TM}CCS_{N2}$ of 468 Å^2, consistent with the experimental value of 476 Å^2. Hence, the reliability of the assignment principle, by comparing experimental and calculated CCS for specific structural models as will be discussed below for the fragments, can be gauged by considering $[Ag_{29}L_{12}]^{3-}$ whose structure is in fact known from single crystal X-ray diffraction.[15] For $[Ag_{29}L_{12}]^{3-}$ we obtained a deviation of 1.7 % (within 2 %). This is our reference for the structural assignments. Since, the fragments $[Ag_{24}L_9]^{2-}$ and $[Ag_{19}L_6]^-$ are similar types of molecules and their structures are calculated using the same method of geometry optimization, similar deviations between experimental and theoretical CCS, i.e. around $\approx \pm 2$ % are also expected. For a well-defined, reasonably rigid molecular ion, a deviation within $\approx \pm 2$ % between experimental and calculated CCS can be considered as good agreement. Figure S7 and Table S1 provide further support for this (and for the applicability of the structure assignment method in general) as obtained from measurements and simulations for a number of other closely related silver clusters.

Two plausible, DFT-based models for the smaller $[Ag_5L_3]^-$ fragment are presented in Figure 3A,B. ^{Ag5}Iso 1 consists of one long Ag–S polymer backbone in which dithiolate ligands form a closed network between the –S binding sites. ^{Ag5}Iso 2 consists of two smaller polymeric units, a cyclic triangular Ag_3S_3 and a short Ag_2S_3 unit, bound together by the dithiols. In both cases, the guiding principle to find the structures was to look for closed systems maintaining the BDT connectivity which maximize the number of Ag–S bonds and avoid steric hindrance of phenyl
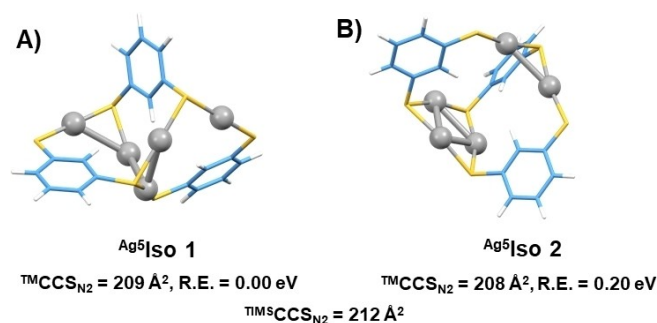
Figure 3. A), B) DFT optimized structures of isomers of $[Ag_5L_3]^-$, (L=1,3-BDT); colours: Ag (grey), S (yellow), C (blue), H (white). Bonds are drawn for Ag–Ag and Ag–S bond lengths less than 3.1 and 2.4 Å, respectively.

rings. $^{TM}CCS_{N2}$ of ^{Ag5}Iso 1 and 2 were 209 and 208 Å^2, respectively, which agreed with $^{TIMS}CCS_{N2}$ of 212 Å^2. Given the small energy difference of 0.20 eV between ^{Ag5}Iso 1 and 2 (Table 1), and the fact that their $^{TM}CCS_{N2}$ values differ by only 1 Å^2, it is not possible to distinguish which of these two structures is observed in experiment based on TIMS alone. Consistent with the relative energy ordering, ^{Ag5}Iso 1 showed slightly better electronic stability with a HOMO–LUMO gap of 2.49 eV compared to 2.17 eV for ^{Ag5}Iso 2 (Table 1). Further dissociation of $[Ag_5L_3]^-$ (Figure S8) showed mainly loss of Ag_2 (and some contribution from Ag–S and C–S

Table 1: Experimental and calculated CCS values, relative energies and HOMO–LUMO gaps of the parent and fragment ions.[a]

Species	Experiment $^{TIMS}CCS_{N2}$ [Å^2]	Calculated $^{TM}CCS_{N2}$ [Å^2] (Isomer.)	Relative energy (R.E.) [eV]/HOMO–LUMO Gap [eV]
$[Ag_{29}L_{12}]^{3-}$	476	468	n.a./1.63
$[Ag_5L_3]^-$	212	1. 209	0.00/2.49
		2. 208	0.20/2.17
$[Ag_{24}L_9]^{2-}$	383	1. **392**	0.36/0.49
		2. 404	0.15/0.50
		3. 424	0.40/0.63
		4. 417	0.00/0.80
		5. 430	0.07/0.84
		6. 415	0.08/0.82
$[Ag_{19}L_6]^-$	303	1. **310**	1.28/1.10
		2. **308**	1.34/1.05
		3. 340	0.90/1.19
		4. 323	0.49/1.23
		5. 328	0.14/1.38
		6. 335	0.00/1.18
		7. 348	2.01/0.61
		8. 330	1.51/0.97
		9. 352	1.09/0.69
		10. 343	0.58/1.30
		11. 336	0.64/1.26
		12. 331	0.41/1.54

[a] $^{TM}CCS_{N2}$ of $[Ag_{29}L_{12}]^{3-}$ and best-fitted fragments, ^{Ag24}Iso 1, ^{Ag19}Iso 2 and ^{Ag5}Iso 2 show linear correlation (slope=0.99) with $^{TIMS}CCS_{N2}$ values indicating that the assigned structures provide a good description of experiment (Figure S15).

Angew. Chem. Int. Ed. **2023**, e202305836 (3 of 6)

© 2023 The Authors. Angewandte Chemie International Edition published by Wiley-VCH GmbH

bond cleavage), suggesting [Ag5]Iso 2 which has distinct motifs containing two, respectively three, Ag atoms may be the isomer formed.

It was significantly more challenging to assign structures for the larger fragment ions $[Ag_{24}L_9]^{2-}$ and $[Ag_{19}L_6]^-$, due to the multitude of possible arrangements of Ag atoms and ligands. One conceivable constraint on the structural space is to regard these fragments as closed shell $8e^-$ superatoms like the parent cluster. Then only structures having compact metallic cores need be considered.[1c,20] In ligand-stabilized clusters of this size, fragmentation is not expected to be a simple one step cleavage process. A cascade of bond rearrangements may occur upon energization.[6,21] However, during the timescale of ≈ 500 ms for the ion mobility measurements carried out at a N_2 pressure of ≈ 2.3 mbar, the activated fragment ions will be quenched back to near room temperature. Keeping these aspects in mind, we constructed a plausible structure for $[Ag_{24}L_9]^{2-}$ by peeling off a suitable number of ligands and Ag atoms from the surface of the parent $[Ag_{29}L_{12}]^{3-}$ cluster and rearranging the remaining motifs to cover the surface. This structure was then optimized by DFT ([Ag24]Iso 1). Structure search was continued by molecular dynamics (MD) simulations beginning with [Ag24]Iso 1 to allow additional dynamic changes and radius of gyration (Rg) was used to follow overall structural fluctuations as shown in Figure 4A. Snapshot structures of $[Ag_{24}L_9]^{2-}$ were selected at various time steps of the MD simulation (corresponding to a range of different Rg values as numbered in Figure 4A) and DFT-optimized to generate more isomeric structures, i.e., [Ag24]Iso 2–[Ag24]Iso 6 (Figure S9),

which showed slight changes in the relative arrangements of atoms in core and staples and reorientations of the ligands compared to [Ag24]Iso 1. HOMO–LUMO gaps of [Ag24]Iso 1–6 (Table 1) show that energetically better isomers have on average larger gaps. For two representative isomers ([Ag24]Iso 1, 6) the projected density of states to spherical harmonics functions (Figure S10A,B) reveals that the lowest unoccupied states are D symmetric matching with the 8e superatom characteristics but the pure P states are missing among the highest occupied states. Delocalized metal core P states are hybridized with other states lower in energy which can be explained by the distorted overall structures of the isomers. [Ag24]Iso 1 showed $^{TM}CCS_{N2}$ of 392 Å^2 which agreed to $^{TIMS}CCS_{N2}$ of 383 Å^2 for $[Ag_{24}L_9]^{2-}$. $^{TM}CCS_{N2}$ of the other isomeric structures of $[Ag_{24}L_9]^{2-}$ were much higher than the experiment (Table 1, Figure S11). [Ag24]Iso 1 was however 0.36 eV higher in energy than the energetically best [Ag24]Iso 4 isomer (Table 1). When an isolated cluster is excited above its dissociation threshold, it may follow a faster, kinetically controlled or a slower, thermodynamically controlled fragmentation channel. The changes in charge distribution as well as ligand-ligand interactions during dissociation may favour kinetically controlled pathways.[22] In this case, fragmentation barriers are conceivably lower than the internal energy barriers for rearrangement to the thermodynamically preferred lowest energy states. Hence, the most stable calculated fragment may not be observed in the experiment. The structure of [Ag24]Iso 1, presented in Figure 4 B,C, consists of an icosahedron core similar to the parent cluster (Figure S12A) with the remaining 11 Ag atoms positioned in the outer staples.

Likewise, for $[Ag_{19}L_6]^-$, two different starting structures were assumed which differed significantly in their size: compact [Ag19]Iso 1 and larger [Ag19]Iso 7, and MD simulations were performed on them. Snapshot structures, denoted as 1–12 in Figure 4D, were similarly selected from the MD runs (i and ii for [Ag19]Iso 1 and [Ag19]Iso 7 initial structures, respectively) and DFT-optimized to generate a set of isomeric structures i.e. [Ag19]Iso 1–[Ag19]Iso 12 (Figure S13). HOMO–LUMO gaps of the Ag$_{19}$ isomers (Table 1) are between 0.61–1.54 eV. The projected density of states of two representative structures, [Ag19]Iso 1,12 (Figure S10C,D) shows that [Ag19]Iso 12 supports better the spherical 8e superatom model as the P and D state symmetries are more pure than for [Ag19]Iso 1. Despite of the icosahedral based, close to spherical metal core, there are variations how strongly the exact structure of metal-ligand interface and structural reconstructions affect the superatom state symmetries. By comparing $^{TM}CCS_{N2}$ of these $[Ag_{19}L_6]^-$ isomers with $^{TIMS}CCS_{N2}$ of 303 Å^2 (Table 1), we find that both [Ag19]Iso 1 and 2 agree with the experiment within 2%. [Ag19]Iso 3–[Ag19]Iso 12 show much higher $^{TM}CCS_{N2}$ (Table 1, Figure S14) and hence can be ruled out. The structure of [Ag19]Iso 2 is presented in Figure 4E,F. Here, the Ag$_{13}$ core forms a highly distorted icosahedron (Figure S12B) and 6 Ag atoms are in the staples. However, both [Ag19]Iso 1 and 2 are significantly higher in energy compared to the lowest energy [Ag19]Iso 6 (Table 1). Again, we interpret this as kinetic control in the dissociation step as already inferred for $[Ag_{24}L_9]^{2-}$. We also
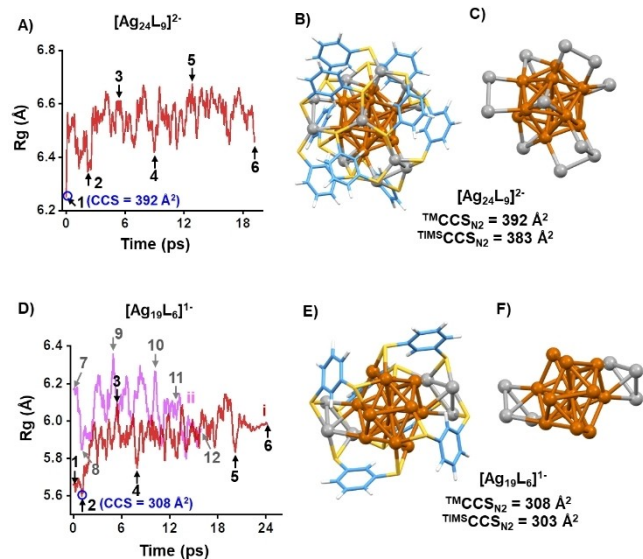
Figure 4. Radius of gyration (Rg) vs time (ps) of MD simulation for A) $[Ag_{24}L_9]^{2-}$ and D) $[Ag_{19}L_6]^-$ (i red and ii pink for two isomers). The numbers in (A) and (D) correspond to different snapshot structures selected from the MD runs at different time of simulation (indicated by arrows). B), E) best fitting structures of $[Ag_{24}L_9]^{2-}$ ([Ag24]Iso 1) and $[Ag_{19}L_6]^-$ ([Ag19]Iso 2) (L=1,3-BDT), respectively; C), F) arrangement of the Ag atoms in [Ag24]Iso 1 and [Ag19]Iso 2, respectively. Color: Ag (orange: core and grey: staple as in parent cluster), S (yellow), C (blue), H (white).

found that the most compact modeled structures of both $[Ag_{24}L_9]^{2-}$ (^{Ag24}Iso 1) and $[Ag_{19}L_6]^-$ (^{Ag19}Iso 1, 2), agree best with the experiment (see Table 1). This supports the exclusion of possible non-superatom structures in the assignment which will have non-spherical shape or less compact cluster cores and hence higher CCS. We note that the calculated fragmentation energies for the stepwise dissociation, $Ag_{29} \rightarrow$ ^{Ag24}Iso 1 + ^{Ag5}Iso 2, and ^{Ag24}Iso 1 $\rightarrow$ ^{Ag19}Iso 2 + ^{Ag5}-Iso 2 were +1.70 eV and +0.38 eV, respectively, i.e. quite low and therefore in support of metal cluster core-staple-ligand shell topologies for both $[Ag_{24}L_9]^{2-}$ and $[Ag_{19}L_6]^-$.

In summary, using TIMS MS and theoretical calculations, we assigned the possible structures of the closed-shell fragments ($[Ag_{24}L_9]^{2-}$, $[Ag_{19}L_6]^-$) and the smaller $[Ag_5L_3]^-$ unit produced upon activation of $[Ag_{29}L_{12}]^{3-}$ in the gas-phase. We showed that $[Ag_{29}L_{12}]^{3-}$ dissociates via two step elimination of $[Ag_5L_3]^-$ to form $[Ag_{19}L_6]^-$, which further dissociates mainly by Ag_2 loss generating species like $[Ag_{17}L_6]^-$, $[Ag_{15}L_6]^-$ and $[Ag_{13}L_6]^-$. Some elimination of a third $[Ag_5L_3]^-$ from $[Ag_{19}L_6]^-$ was also observed. This would nominally generate neutral $[Ag_{14}L_3]$ that could be probed by UV photoionization MS in future. In condensed phase, the known 1,3-BDT stabilized Ag clusters are $[Ag_{51}L_{19}]^{3-}$[23] and $[Ag_{29}L_{12}]^{3-}$.[15] By contrast, the known clusters synthesized using 1,2-BDT, an analogous dithiol with smaller bite angle, are $[Ag_{14}(1,2\text{-BDT})_6(PPh_3)_8]$[24] and $[Ag_9(1,2\text{-BDT})_6]^{3-}$,[25] i.e. with significantly smaller cores. This trend combined with our observations argues that the gas-phase fragmentation dynamics of $[Ag_{29}L_{12}]^{3-}$ reflects a competition between electronic stability of the Ag cluster core and increasing steric strain of ligands as the nuclearity is reduced. The first two fragmentation steps appear simply to shrink the cluster while keeping its overall compact core-staple-ligand topology intact. Eventually, a still smaller 8e superatom core cannot be maintained without relaxing the connectivity of the remaining dithiol ligands which leads instead to further loss of small neutral fragments. How would fragmentation in condensed phase/solution compare to this? In solution, multiply charged cluster ions are stabilized by interactions with the solvent molecules. These are completely absent in gas-phase and consequently isolated multianions can have very different decay channels such as scission into two anionic fragments (as observed here) and electron (auto)detachment[26] (not observed). Thus, collisional activation can form reactive fragment ions, which are not accessible in solution. Such fragments may in turn be mass selected and softly deposited onto surfaces[27] to study e.g. their catalytic behavior compared to the parent clusters (whose active centers are better shielded from the reagents by (more) ligands).[28] Hence, resolving the fragment structures obtained upon $[Ag_{29}L_{12}]^{3-}$ activation in gas phase as done here will also prove useful for future model catalysis probes.

Conflict of Interest

The authors declare no conflict of interest.

Data Availability Statement

The data that support the findings of this study are available from the corresponding author upon reasonable request.

[1] a) R. Jin, C. Zeng, M. Zhou, Y. Chen, *Chem. Rev.* **2016**, *116*, 10346–10413; b) I. Chakraborty, T. Pradeep, *Chem. Rev.* **2017**, *117*, 8208–8271; c) M. Walter, J. Akola, O. Lopez-Acevedo, P. D. Jadzinsky, G. Calero, C. J. Ackerson, R. L. Whetten, H. Grönbeck, H. Häkkinen, *Proc. Natl. Acad. Sci. USA* **2008**, *105*, 9157–9162.

[2] a) P. Chakraborty, A. Baksi, E. Khatun, A. Nag, A. Ghosh, T. Pradeep, *J. Phys. Chem. C* **2017**, *121*, 10971–10981; b) L. A. Angel, L. T. Majors, A. C. Dharmaratne, A. Dass, *ACS Nano* **2010**, *4*, 4691–4700.

[3] G. E. Johnson, T. Priest, J. Laskin, *Chem. Sci.* **2014**, *5*, 3275–3286.

[4] D. M. Black, C. M. Crittenden, J. S. Brodbelt, R. L. Whetten, *J. Phys. Chem. Lett.* **2017**, *8*, 1283–1289.

[5] X. Kang, H. Chong, M. Zhu, *Nanoscale* **2018**, *10*, 10758–10834.

[6] C. Liu, S. Lin, Y. Pei, X. C. Zeng, *J. Am. Chem. Soc.* **2013**, *135*, 18067–18079.

[7] K. Michelmann, J. A. Silveira, M. E. Ridgeway, M. A. Park, *J. Am. Soc. Mass Spectrom.* **2015**, *26*, 14–24.

[8] a) D. E. Clemmer, M. F. Jarrold, *J. Mass Spectrom.* **1997**, *32*, 577–592; b) Y. Mao, M. A. Ratner, M. F. Jarrold, *J. Phys. Chem. B* **1999**, *103*, 10017–10021.

[9] F. Hennrich, E. Schneider, P. Weis, M. M. Kappes, *J. Am. Soc. Mass Spectrom.* **2019**, *30*, 1973–1980.

[10] a) A. Baksi, A. Ghosh, S. K. Mudedla, P. Chakraborty, S. Bhat, B. Mondal, K. R. Krishnadas, V. Subramanian, T. Pradeep, *J. Phys. Chem. C* **2017**, *121*, 13421–13427; b) E. Kalenius, S. Malola, M. F. Matus, R. Kazan, T. Bürgi, H. Häkkinen, *J. Am. Chem. Soc.* **2021**, *143*, 1273–1277; c) K. Hirata, P. Chakraborty, A. Nag, S. Takano, K. Koyasu, T. Pradeep, T. Tsukuda, *J. Phys. Chem. C* **2018**, *122*, 23123–23128; d) C. Comby-Zerbino, F. Bertorelle, P. Dugourd, R. Antoine, F. Chirot, *J. Phys. Chem. A* **2020**, *124*, 5840–5848.

[11] a) A. Baksi, E. K. Schneider, P. Weis, K. R. Krishnadas, D. Ghosh, H. Hahn, T. Pradeep, M. M. Kappes, *J. Phys. Chem. C* **2019**, *123*, 28477–28485; b) A. Baksi, E. K. Schneider, P. Weis, I. Chakraborty, O. Fuhr, S. Lebedkin, W. J. Parak, M. M. Kappes, *ACS Nano* **2020**, *14*, 15064–15070.

[12] S. Daly, C. M. Choi, A. Zavras, M. Krstić, F. Chirot, T. U. Connell, S. J. Williams, P. S. Donnelly, R. Antoine, A. Giuliani, V. Bonačić-Koutecký, P. Dugourd, R. A. J. O'Hair, *J. Phys. Chem. C* **2017**, *121*, 10719–10727.

[13] A. Soleilhac, F. Bertorelle, C. Comby-Zerbino, F. Chirot, N. Calin, P. Dugourd, R. Antoine, *J. Phys. Chem. C* **2017**, *121*, 27733–27740.

[14] M. R. Ligare, K. A. Morrison, M. A. Hewitt, J. U. Reveles, N. Govind, H. Hernandez, E. S. Baker, B. H. Clowers, J. Laskin, G. E. Johnson, *J. Phys. Chem. Lett.* **2021**, *12*, 2502–2508.

[15] L. G. AbdulHalim, M. S. Bootharaju, Q. Tang, S. Del Gobbo, R. G. AbdulHalim, M. Eddaoudi, D.-e. Jiang, O. M. Bakr, *J. Am. Chem. Soc.* **2015**, *137*, 11970–11975.

[16] D. Morsa, E. Hanozin, G. Eppe, L. Quinton, V. Gabelica, E. D. Pauw, *Anal. Chem.* **2020**, *92*, 4573–4582.

[17] J. Enkovaara, C. Rostgaard, J. J. Mortensen, J. Chen, M. Dułak, L. Ferrighi, J. Gavnholt, C. Glinsvad, V. Haikola, H. A. Hansen, H. H. Kristoffersen, M. Kuisma, A. H. Larsen, L. Lehtovaara, M. Ljungberg, O. Lopez-Acevedo, P. G. Moses, J. Ojanen, T. Olsen, V. Petzold, N. A. Romero, J. Stausholm-Møller, M. Strange, G. A. Tritsaris, M. Vanin, M. Walter, B. Hammer, H. Häkkinen, G. K. Madsen, R. M. Nieminen, J. K. Nørskov, M. Puska, T. T. Rantala, J. Schiøtz, K. S. Thygesen, K. W. Jacobsen, *J. Phys. Condens. Matter* **2010**, *22*, 253202.

[18] J. P. Perdew, K. Burke, M. Ernzerhof, *Phys. Rev. Lett.* **1996**, *77*, 3865–3868.

[19] C. Larriba, C. J. Hogan, Jr., *J. Phys. Chem. A* **2013**, *117*, 3887–3901.

[20] W. D. Knight, K. Clemenger, W. A. de Heer, W. A. Saunders, M. Y. Chou, M. L. Cohen, *Phys. Rev. Lett.* **1984**, *52*, 2141–2143.

[21] P. Chakraborty, A. Nag, G. Natarajan, N. Bandyopadhyay, G. Paramasivam, M. K. Panwar, J. Chakrabarti, T. Pradeep, *Sci. Adv.* **2019**, *5*, eaau7555.

[22] M. R. Ligare, J. U. Reveles, N. Govind, G. E. Johnson, J. Laskin, *J. Phys. Chem. C* **2019**, *123*, 24899–24911.

[23] A. Ghosh, D. Ghosh, E. Khatun, P. Chakraborty, T. Pradeep, *Nanoscale* **2017**, *9*, 1068–1077.

[24] M. Bodiuzzaman, E. Khatun, K. S. Sugi, G. Paramasivam, W. A. Dar, S. Antharjanam, T. Pradeep, *J. Phys. Chem. C* **2020**, *124*, 23426–23432.

[25] B. J. Alamer, M. S. Bootharaju, S. M. Kozlov, Z. Cao, A. Shkurenko, S. Nematulloev, P. Maity, O. F. Mohammed, M. Eddaoudi, L. Cavallo, J.-M. Basset, O. M. Bakr, *Inorg. Chem.* **2021**, *60*, 4306–4312.

[26] M. N. Blom, O. Hampe, S. Gilb, P. Weis, M. M. Kappes, *J. Chem. Phys.* **2001**, *115*, 3690–3697.

[27] H. Y. Samayoa-Oviedo, K.-A. Behrend, S. Kawa, H. Knorke, P. Su, M. E. Belov, G. Anderson, J. Warneke, J. Laskin, *Anal. Chem.* **2021**, *93*, 14489–14496.

[28] a) Y. Negishi, N. Shimizu, K. Funai, R. Kaneko, K. Wakamatsu, A. Harasawa, S. Hossain, M. E. Schuster, D. Ozkaya, W. Kurashige, T. Kawawaki, S. Yamazoe, S. Nagaoka, *Nanoscale Adv.* **2020**, *2*, 669–678; b) C. Garcia, V. Truttmann, I. Lopez, T. Haunold, C. Marini, C. Rameshan, E. Pittenauer, P. Kregsamer, K. Dobrezberger, M. Stöger-Pollach, N. Barrabés, G. Rupprechter, *J. Phys. Chem. C* **2020**, *124*, 23626–23636.

Communications

Silver Clusters

P. Chakraborty,* S. Malola, M. Neumaier,
P. Weis, H. Häkkinen,*
M. M. Kappes* ————— **e202305836**

Elucidating the Structures of Intermediate
Fragments during Stepwise Dissociation of
Monolayer-Protected Silver Clusters

$[Ag_{29}L_{12}]^{3-}$ ——— $[Ag_{24}L_9]^{2-}$ ——— $[Ag_{19}L_6]^{1-}$

stepwise loss of $[Ag_5L_3]^-$
structure determination by ion mobility

$[Ag_{29}L_{12}]^{3-}$ $[Ag_{24}L_9]^{2-}$ $[Ag_{19}L_6]^{1-}$ $[Ag_5L_3]^{1-}$

500   400   300   200
$^{TIMS}CCS_{N2}$ (Å^2)
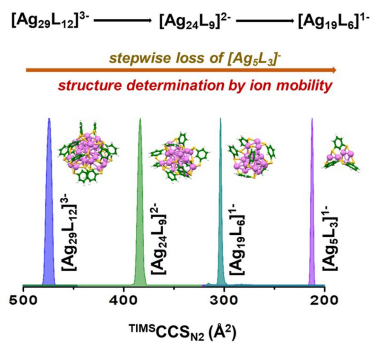
Trapped ion mobility mass spectrometry, combined with theoretical calculations, is used to resolve the structures of intermediate fragments produced upon dissociation of atomically precise silver clusters in the gas-phase, which has remained challenging using other methodologies.